Translational Research xxx (xxxx) xxx

Contents lists available at ScienceDirect

Translational Research

journal homepage: www.elsevier.com/locate/trsl

Efficacy of oral manganese and D-galactose therapy in a patient bearing a novel TMEM165 variant

Zoé Durin [a,1], Alexandre Raynor [b,1], François Fenaille [c], Sophie Cholet [c], Sandrine Vuillaumier-Barrot [b,d], Jean-Meidi Alili [e], Joël Poupon [f], Nouzha Djebrani Oussedik [f], Caroline Tuchmann-Durand [g], Jennifer Attali [h], Romain Touzé [i], Thierry Dupré [b], Elodie Lebredonchel [b], Marlyse Angah Akaffou [b], Dominique Legrand [a], Pascale de Lonlay [e,j,2,***], Arnaud Bruneel [b,k,2,**], François Foulquier [a,2,*]

[a] Univ. Lille, CNRS, UMR 8576 – UGSF - Unité de Glycobiologie Structurale et Fonctionnelle, F-59000 Lille, France
[b] AP-HP, Biochimie Métabolique et Cellulaire, Hôpital Bichat-Claude Bernard, 46 rue Henri Huchard, 75018 Paris, France
[c] Université Paris-Saclay, CEA, INRAE, Département Médicaments et Technologies pour la Santé (DMTS), MetaboHUB, 91191 Gif sur Yvette, France
[d] Laboratoire de biologie médicale multisites Seqoia - FMG2025, 75014 Paris, France
[e] Filière G2m, Hôpital Universitaire Necker-Enfants-Malades, Assistance Publique-Hôpitaux de Paris (AP-HP), 75015 Paris, France
[f] Laboratoire de Toxicologie biologique Groupe hospitalier Saint Louis - Lariboisière - Fernand Widal, 75475, Paris, France
[g] Institut Imagine, Biothérapie, Hôpital Universitaire Necker-Enfants-Malades, Assistance Publique-Hôpitaux de Paris (AP-HP), Institut Imagine, 75015 Paris, France
[h] Service de Radiologie Pédiatrique, Hôpital Universitaire Necker-Enfants-Malades, Assistance Publique-Hôpitaux de Paris (AP-HP), Institut Imagine,75015 Paris, France
[i] Service d'Ophtalmologie Pédiatrique, Hôpital Universitaire Necker-Enfants-Malades, Assistance Publique-Hôpitaux de Paris (AP-HP), 75015 Paris, France
[j] Hôpital Universitaire Necker-Enfants-Malades, Institut Imagine, G2M, MetabERN, Université Paris Cité, 75015 Paris, France
[k] INSERM UMR1193, Faculté de Pharmacie, Université Paris-Saclay, bâtiment Henri Moissan, 92400 Orsay, France

ARTICLE INFO

Keywords:
TMEM165
Manganese
galactose
Golgi
Glycosylation

ABSTRACT

TMEM165-CDG has first been reported in 2012 and manganese supplementation was shown highly efficient in rescuing glycosylation in isogenic KO cells. The unreported homozygous missense c.928G>C; p.Ala310Pro variant leading to a functional but unstable protein was identified. This patient was diagnosed at 2 months and displays a predominant bone phenotype and combined defects in *N-*, *O-* and GAG glycosylation. We administered for the first time a combined D-Gal and Mn^{2+} therapy to the patient. This fully suppressed the N-; O- and GAG hypoglycosylation. There was also striking improvement in biochemical parameters and in gastrointestinal symptoms. This study offers exciting therapeutic perspectives for TMEM165-CDG.

Introduction

Congenital Disorders of Glycosylation (CDG) have been first clinically reported in 1980. To date some 160 different genes involved CDG are currently known.[1,2] TMEM165-CDG, first reported in 2012 is a defect in Ca/Mn Golgi homeostasis[3] and TMEM165-CDG patients show important skeletal abnormalities including dwarfism, osteoporosis, scoliosis and joint laxity.[3,4] Four pathogenic variants have been reported in seven patients: three homozygous variants c.792+182 G>A (activation of a cryptic splice donor site), two missense variants c.377G>A and c.332A>G respectively and one compound heterozygous variant c.377C>T and c.910G>A. TMEM165-CDG is unique and leads to hypogalactosylation of four Golgi glycosylation pathways: *N*-glycosylation, *O*-glycosylation, GAG and glycolipids synthesis.[5,6] The link between TMEM165 and Golgi Mn^{2+} homeostasis came from the observation that Mn^{2+} supplementation fully rescues the glycosylation defects in TMEM165-KO cells. Moreover, the stability of TMEM165 is Mn^{2+}-dependent as increasing Mn^{2+} concentrations target TMEM165

* Corresponding author at: CNRS, UMR 8576 - Unité de Glycobiologie Structurale et Fonctionnelle, Lille, France.
** Co-corresponding author at: AP-HP, Biochimie Métabolique et Cellulaire, Hôpital Bichat-Claude Bernard, 46 rue Henri Huchard, 75018 Paris, France.
*** Co-corresponding author at: Hôpital Universitaire Necker-Enfants-Malades, Institut Imagine, G2M, MetabERN; Université Paris Cité, 75015 Paris, France.
E-mail addresses: pascale.delonlay@aphp.fr (P. de Lonlay), arnaud.bruneel@aphp.fr (A. Bruneel), francois.foulquier@univ-lille.fr (F. Foulquier).
[1] These authors contributed equally
[2] These authors contributed equally

https://doi.org/10.1016/j.trsl.2023.11.005
Received 17 July 2023; Received in revised form 6 November 2023; Accepted 17 November 2023
Available online 25 November 2023
1931-5244/© 2023 The Author(s). Published by Elsevier Inc. This is an open access article under the CC BY-NC-ND license (http://creativecommons.org/licenses/by-nc-nd/4.0/).

for lysosomal degradation.[7]

Still very few CDG are treatable with a specific drug (e.g. mannose in MPI-CDG; D-Galactose (D-Gal) in SLC35A2-CDG and PGM1-CDG).[8–12] The oral supplementation with these monosaccharides improved patient symptoms, with a very low risk of secondary effects and D-Galactose (D-Gal) supplementation has been shown very efficient to rescue the *N*-glycosylation defects. Two TMEM165-CDG patients treated with D-Gal improved their N-glycosylation.[13] However, our recent results in TMEM165-KO cells demonstrated that D-Gal supplementation could only rescue the *N*-glycosylation defects whereas Mn^{2+} supplementation could rescue all the glycosylation defects.[5] We report a 2 months-old TMEM165-CDG patient with a novel homozygous variant. She presented with hypovolemic shocks due to gastroenteritis in the first months of life, diarrhea, failure to thrive, skeletal abnormalities, liver cytolysis and abnormal hemostasis as well as discrete combined serum *N*- and *O*-linked hypoglycosylation. We started treatment with $MnSO_4$ and D-galactose and report here the clinical and biochemical evolution during 1 year follow-up under this treatment.

Materials and methods

Patient

Ethics

Approval of the local Ethics Committee, the CERAPHP (*Comité d'Ethique pour la Recherche AP-HP*), to treat this patient with the manganese-galactose association, off-label, on a compassionate basis was obtained (IRB registration: #00011928). We collected consent form from parents for the treatment on a compassionate basis and a non-opposition for data publication including the picture of the patient.

Manganese and galactose treatment

Oral manganese element (Mn) using manganese sulphate monohydrate salt, $MnSO_4.H_2O$ in magistral preparation, was introduced and progressively increased from 2 mg/day to 10 mg/Kg/day. D-Galactose (D-Gal, magistral preparation) was progressively increased from 4 g to 12g/day.

Serum glycosylation studies

Transferrin N-glycosylation

Capillary electrophoresis of Tf was performed as previously described on a Capillarys 2 Flex Piercing (CDT kit, ref 2009; Sebia, France).[14]

Analysis of total serum N-glycans by matrix-assisted laser desorption/ionization time-of-flight mass spectrometry (MALDI-TOF MS)

Total serum *N*-glycan profiles were studied by MALDI-TOF MS following *N*-glycan cleavage by peptide *N*-glycosidase F (PNGase F from Roche Diagnostics (100 U, lyophilized, product reference 11 365 185 001, Mannheim, Germany)), glycan purification by solid-phase extraction and permethylation as previously described in.[15,16] The MALDI-TOF mass spectra were internally calibrated, and further processed using the GlycoWorkBench software.[17]

Mucin core 1 O-glycosylation

2-DE of apoC-III was performed as previously described.[18] Primary antibody (rabbit anti-apoC-III cat #K97113R, 1:5000 v/v in 5% TBST; Meridian Bioscience, USA), and then with the secondary antibody (goat anti-rabbit HRP-conjugated IgG NA934V, Biorad, 1:5000 v/v).

Glycosaminoglycans

Western blot of bikunin was performed as previously described.[19] Primary antibody (rabbit anti-bikunin (CP6) polyclonal antibody cat #ATB1346, 1:5000 v/v in 5% TBST milk; Merck-Millipore, USA) and then with the secondary antibody (goat anti-rabbit HRP-conjugated, 1:5000 v/v, GE Healthcare).

Cell studies

Cell culture & reagent

Patient and gender matched control fibroblasts (below 5 years old) were cultured in Dulbecco's Modified Eagle's Medium (DMEM) (Lonza, Basel, Switzerland) supplemented with 10% fetal bovine serum (#50010551, PAN Biotech, Germany) and maintained at 37°C in humidity-saturated and 5% CO_2 atmosphere. When indicated, cells were treated with 2.5 μM of $MnCl_2$ (CAS: 13446-34-9, Riedel-de-Haën, Seelze, Germany) or 100 μM chloroquine (#C6628, Sigma-Aldrich, St Louis, MO, USA).

Western-blot analysis

Western-blot analysis was performed as previously described. Briefly the cells were washed three time and scrapped in Dulbecco's Phosphate Buffer (DPBS, Lonza) and then centrifuged at 6000 rpm, 4°C for 10 min. Supernatant was eliminated, and cell pellets were resuspended with RIPA buffer [Tris/HCl 50 mM pH 7.9, NaCl 120 mM, NP40 0.5%, EDTA 1 mM, Na_3VO_4 1 mM, NaF 5 mM] supplemented with a protease inhibitor cocktail (#11697498001 Roche Diagnostics, Penzberg, Germany). Cells were lysed and centrifugated at 20000g, 4°C for 30 min. Protein concentration in the supernatant was estimated with the micro–BCA Protein Assay Kit (# 10249133, Thermo Fischer Scientific, Waltham, MA United States). 10 μg of protein were mixed with Laemmli buffer (for TMEM165 Western-blotting) or NuPAGE Lithium Dodecyl Sulfate (LDS) Sample Buffer (Fisher Scientific, Waltham, USA), pH 8.4, supplemented with 4% β-mercaptoethanol (Fluka). For TGN46 and LAMP2 analysis, samples were denaturated for 10 min at 95°C, separated on 4%–12% Bis-Tris gels (#NP0322BOX Invitrogen), and for TMEM165, samples were not heated and separated on a home-cast 12% gel. β-actin antibody was purchased from MilliporeSigma (Burlington, MA, United States) and used at 1:10000 v/v dilutions. TMEM165 antibodies were purchased fromMilliporeSigma (Ref HPA038299 #000028770) and used at 1:3000 v/v dilution. Mouse anti-LAMP2 antibody from Santa Cruz Biotechnology (#H4B4, sc-188822, Dallas, TX, United States) was diluted at 1:2000 and sheep anti-TGN46 (#AHP500G, Biorad) at 1:1000 v/v. Secondary antibodies (HRP-coupled) were purchased from MilliporeSigma (#12-348 and #12-349) and used at 1/10000 v/v dilutions.

Immunofluorescence

Cells were seeded on glass coverslips in 6-well plates and incubated in the above-described cell culture conditions for 48 h. Cells were then washed three times with Dulbecco's Phosphate Buffer Saline containing magnesium and calcium (DPBS+/+) (Sigma Aldrich) and fixed with 4% paraformaldehyde for 20 min at room temperature. Coverslips were then washed three times with PBS and cells were permeabilized with 0.5% Triton X-100 in PBS for 10 min before three washes with PBS. Coverslips were then incubated for 1h in blocking buffer [0.2% gelatin, 2% Bovin Serum Albumin (BSA), 2% Fetal Bovine Serum (FBS) (Lonza) in PBS] and then for 1 h with primary antibody diluted at 1:100 in blocking buffer. After three washing with PBS, cells were incubated for 1h with Alexa 488- or Alexa 568-conjugated secondary antibody (GAM-488 #10138324 and GAR-568 #10463022 Life Technologies) diluted at 1:600 in blocking buffer. After three washes with PBS, coverslips were mounted on glass slides with Mowiol. Fluorescence was detected through an inverted Zeiss LSM780 or LSM700 confocal microscope. Acquisitions were done using the ZEN pro 2.1 software (Zeiss, Oberkochen, Germany).

Image analyses

Immunofluorescence images were analyzed and quantified using imageJ (http://imagej.nih.gov/ij).

Genetic studies

Whole genome sequencing

Quantification and qualification of nucleic acids are respectively obtained on Spark, TECAN and Fragment Analyzer, Agilent. The fragments are generated by sonication (LE220plus, Covaris). The size selection, like the subsequent purification steps, are carried out on magnetic beads (Sera-Mag magnetic beads, cat# 21152104011150; GE Healthcare). The preparation of the library is carried out without amplification (NEBNext Ultra II End repair/A-tailing module & Ligation module, NEB#E7546S, NEB #E7595 New England Biolabs). The library is quantified by qPCR (NEBNext Custom 2X Library Quant Kit Master Mix, New England Biolabs cat#E7630S; QuantStudio 6 Flex Real-Time PCR System, Life Technologies). The libraries are sequenced in 'paired-end' (2 times 150 cycles) by SBS technology (Flow Cell S4, NovaSeq 6000, Illumina).

Bioinformatics analysis

Sequence files are demultiplexed. The alignment of the files obtained on the reference genome (GRCh38) uses a Burrows-Wheeler transform (BWA-MEM). The marking of duplicates is done by Picard MarkDuplicates, the recalibration of the base quality score is performed by GATK4 (Broad Institute) and then annotated using SNPeff and SnpSift: the databases queried are as follows: SNPEff, 1000Genomes, gnomAD, ClinVar, COSMIC, dbscSNV, dbSNP, dbNSFP, phastCons. CNV calling is done by CNVnator (Mark B. Gerstein lab, Yale University) and annotation is done by AnnotSV.

Sanger confirmation

NGS findings were confirmed by Sanger sequencing of PCR products amplified from the genomic DNA surrounding each respective variant. Purification of amplicons was performed using the PureIT ExoZAP procedure before sequencing with the Big Dye Terminator Cycle Sequencing System v3.1 (Applied Biosystems) on an ABI PRISM 3100 Genetic Analyzer (Applied Biosystems).

Tools for predicting protein and peptide structures

Model of the Δ80-TMEM165 with the variant A310P was produced with a locally-installed version of the AlphaFold v2.2 software,[20] as previously described in.[21] The models shown in the figures were rendered with the UCSF ChimeraX v1.6 software (https://www.cgl.ucsf.edu/chimerax/). The Orientations of Proteins in Membranes (OPM) database (https://opm.phar.umich.edu/) has been used to calculate the spatial arrangement of the AF2-predicted models with respect to the hydrocarbon core of the lipid bilayer.[22]

For the prediction of peptide structures shown in Supplementary Fig. 2, both AlphaFold 2 and ESMFold [22] were used by the mean of the integrated structure features of ChimeraX v1.6 through the Colab network.[23]

Results

Clinical presentation of the patient

The patient, a girl is the only child of first cousin parents of Kabyle origin. She was born at term by breech Caesarean section, with intrauterine growth retardation (weight 2670 g; height 47.5 cm; head circumference 34.5 cm). There were no difficulties in the neonatal period. From birth to 3 months old, the feeding was mixed, including breast-feeding and infant formula; thereafter, the feeding only comprised formula. Early complications included an E. coli pyelonephritis and diarrhea with 5 then 15 liquid stools per day. At the age of 2 and 3 months, she presented two hypovolemic shocks due to gastroenteritis, related to rotavirus and enterovirus, respectively. A milk without cow protein was introduced and the clinical evolution was considered favorable. However, after these digestive episodes, a stagnation in weight and height was noted (weight and height at -1.5 SD at 6 months, -2 SD from 7 to 12 months, -3 SD at 14 months) with a normal head circumference, related to a failure to thrive. At the age of 9 months, clinical examination showed mild facial dysmorphism (Fig. 1A), a nystagmus with a good eye tracking, a discreet delay in psychomotor development, a clinical hepatomegaly, equinovarus foot and an atopic dermatitis were noted. She had a second episode of pyelonephritis at the age of 12 months and a fracture of the left femur after a fall at the age of 15 months. The psychomotor evaluation (Bayley 3 - Scales of infant and toddler development) performed at the age of 12 months prior to treatment revealed a normative cognitive development, but language and fine motor domains were at the limit of the norm, and global motor skills showed a significative delay for her age (Cognitive 100, Language 77, Motor 64). The child had very good contact, good eye tracking, smile-response, sitting acquired from 5 1/2 months of age. At 8 months of age, she was reaching for objects, passing them from one hand to the other. At 14 months, she could stand with support and eat with her hands.

Scans of the spine, pelvis, left arm and left knee were performed at 12 months, and showed an important bone demineralization and vertebral collapses resulting in a loss of vertebral body height and osteocondensation of the vertebral plates (Fig. 1B). Calcium and phosphate dosages were normal. Ophthalmological examination revealed a hyperopia, normal anterior segment, a bilateral macular pseudohole on the fundus with normal optic nerves. Macular optical coherence tomography (OCT) showed a small bilateral serous retinal detachment under the fovea which extends temporally. An examination under anesthesia was performed with normal retinal fluorescein angiography, normal electroretinogram and visual evoked potentials. All ocular explorations did not account for this phenotype. Genetic testing with a limited panel of 90 genes involved in retinal dystrophies was negative.

At the ages of 3, 9 and 11 months, laboratory examinations revealed a hepatic cytolysis with increased AST and ALT (ALT decreased to reach quasi normal values), variable blood albumin levels, abnormal hemostasis parameters including factor XI, antithrombin (AT), protein C, protein S, and a mild increase of blood creatine kinase (CK) levels (Supp Table 1). Prothrombin time was normal, as well as factors II, V and VII initially. These last proteins decreased when the patient was 11 months (Suppl Table 1). Vitamin K was administered. There was also minimal tubular proteinuria requiring no treatment or supplementation, with progressive improvement, and a normal renal ultrasound.

The association of hemostasis disorders and hepato-digestive disorders led us to investigate a potential CDG.

Worsening of initial N-glycosylation defects after breastfeeding cessation

Following the first consultation, *N*-glycosylation analysis of the patient (at the age of 3 months, serum sample S1) showed a discrete type-2 serum transferrin profile compared to control (Fig. 1C). One month later (S2), a dramatically-altered Tf profile with a marked decrease % of 4-sialoTf (8.8%; N = 78-86%) together with a concomitant increase % of all hyposialylated Tf glycoforms was observed. Intriguingly, this major worsening of *N*-glycosylation was consecutive to breastfeeding cessation.

To investigate the nature of the *N*-glycosylation defects, analysis of the total serum *N*-glycome was performed using MALDI-TOF MS (Fig 1. D). Remarkably, the *N*-glycan profile of the patient at 4 months (S2) appears drastically different from both the control and S1 *N*-glycan patterns from the patient (at 3 months old), with an almost total absence of tri- and tetra-antennary structures and a marked accumulation of truncated structures lacking sialic acid and galactose residues (e.g. *m/z* 1661.8, 1865.9, 2081.0, 2227.1, 2431.2 and 2605.3) (Fig. 1D).

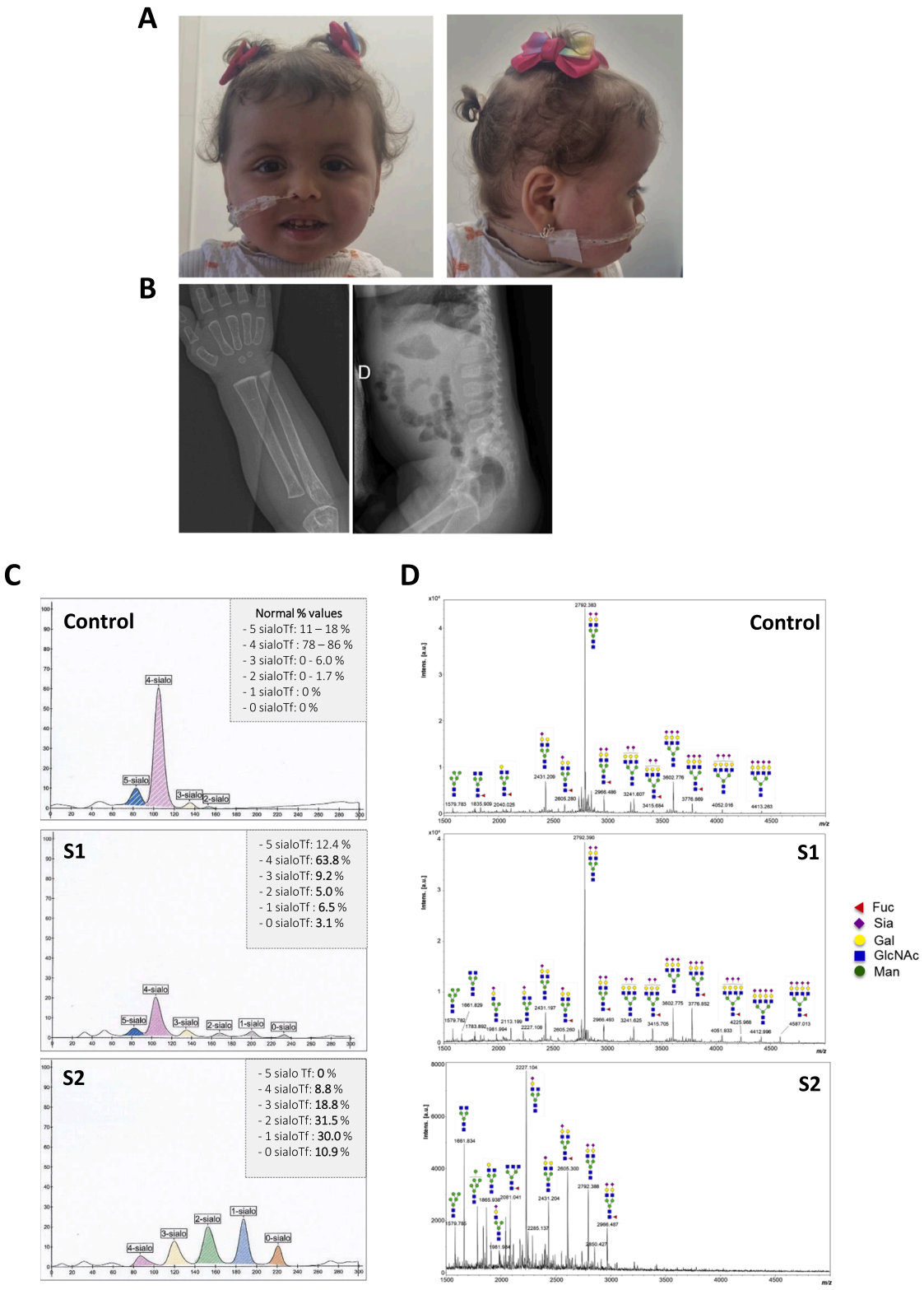

Fig. 1. Clinical presentation of the patient, and initial *N*-glycosylation defects

A. Face: Large, broad forehead, thick eyebrows and synophris, retraction of columella, epicanthus, upper lip finer than lower lip. Profile: rounded forehead, pronounced nasal ensellure, long eyelashes. **B.** left arm radiography and spine radiography at one year, prior to treatment (upper images). **C.** Capillary electrophoresis of serum Tf in control and patient (3 months and 4 months old respectively). **D.** MALDI-TOF mass spectra of PNGase F-released permethylated total serum *N*-glycans from control and patient (3 months and 4 months old). Measurements were performed in the positive-ion mode and all ions are present in sodiated [M+Na+] form. Green circles, mannose (Man); yellow circles, galactose (Gal); blue squares, N-acetylglucosamine (GlcNAc); red triangles, fucose (Fuc); purple diamonds, sialic acid (Sial).

Identification of a novel homozygous missense variant in the human TMEM165 gene and predicted impact of the variant on the protein structure

The observed galactosylation defect led us to investigate a potential TMEM165 deficiency. The index case and both parents were investigated using whole genome sequencing (WGS). A class IV missense variant: Chr4 (GRCh38:g.55425405G>C; ENST00000381334.9 (TMEM165):c.928G>C;p.Ala310Pro), was detected at the homozygous state in the exon 6 of *TMEM165* (NM_018475.5) and absent in GnomAD. NGS findings were confirmed by Sanger sequencing (Fig. 2A). The parents are healthy heterozygous carriers.

Interestingly, amino acid residue 310 of TMEM165 is located within the sixth transmembrane domain (TMD 6) of the protein whose AlphaFold 2 (AF2)-predicted structure was reported recently.[21] Fig. 2B shows a model of the TMEM165-A310P protein generated by AF2. As shown, the A310P variant is far from both conserved E-ϕ-G-D-K/R-T/S motifs important for the transport of Mn^{2+} in the Golgi[21] and no obvious difference with the model without variant was observed. To further analyze the impact of the mutation on TMEM165 structure, both AF2 and EMSFold predictions were generated on peptides encompassing the sole amino-acid residues of TMD 6 (Supp Fig. 1). Results show that the A310P variant causes a deformation of TMD 6 that could affect the position and/or structural conformation of TMD 3 and possibly that of the whole protein.

Mutated TMEM165-A310P protein is unstable

To assess the effect of the A310P variant on TMEM165 protein level, we first performed immunoblots with protein lysates of fibroblasts from patient and control. Reduced level of mutated TMEM165 (70% decrease compared to control) was identified (Fig. 3A). Immunofluorescence confocal microscopy confirmed the western blot result. While TMEM165 perfectly colocalizes with the GM130 Golgi marker in control fibroblasts, a complete absence of TMEM165 in the Golgi could be seen in patients' fibroblasts (Fig. 3B). Quantification of confocal images indicates +/- 3% of residual Golgi TMEM165 in patient's cells compared to control (Fig. 3B). Altogether these results demonstrate a marked destabilization of the variant p.Ala310Pro *in vivo*.

Mutated TMEM165-A310P protein is functional

The functional impact of the A310P variant on TMEM165 was assessed by the ability of the mutated form of TMEM165 to rescue the glycosylation defect of LAMP2, used as a *N*-glycosylation marker in TMEM165 KO HEK293T cells. Unlike untransfected cells (KO), cells expressing the wt-TMEM165 fully rescue LAMP2 glycosylated forms. Intriguingly, the expression of the A310P mutated form of TMEM165 shows identical results with a complete suppression of the LAMP2 glycosylation defects. The expression level of the mutated form was then followed by Western-blot experiments. Although the wt-TMEM165 is well expressed, a strong decrease in expression level of the A310P mutated form was observed (Fig. 3C). These results demonstrate that the A310P mutated form, although unstable, is fully functional in rescuing the glycosylation defects.

Degradation of the TMEM165-A310P protein is inhibited by chloroquine

Our previous results thoroughly established that the turnover of TMEM165 is inhibited by chloroquine treatment.[7] To assess whether the A310P mutated form of TMEM165 falls under the same regulation, the stability of wt- and mutated forms of TMEM165 were analyzed by immunofluorescence in the presence or the absence of chloroquine (Cq). In control fibroblasts, chloroquine treatment led to a slightly higher TMEM165 immunofluorescence signal arguing for an inhibition of its lysosomal degradation. Very interestingly, the same treatment in the patient's fibroblasts fully rescued the TMEM165 expression level and its Golgi subcellular localization as proved by its colocalization with GM130 (Fig. 4A). Proteasomal inhibition did not rescue TMEM165 expression (data not shown). Therefore, chloroquine slowed down the turnover of the mutated TMEM165-A310P protein more efficiently than for the wild type form. These results fully demonstrate that, unlike to wt-TMEM165, the TMEM165 A310P mutated form is unstable due to its higher lysosomal–dependent degradation.

Both manganese and chloroquine treatments rescue the TGN46 glycosylation in the patient's cells

Supplementation of tiny $MnCl_2$ concentrations on the suppression of

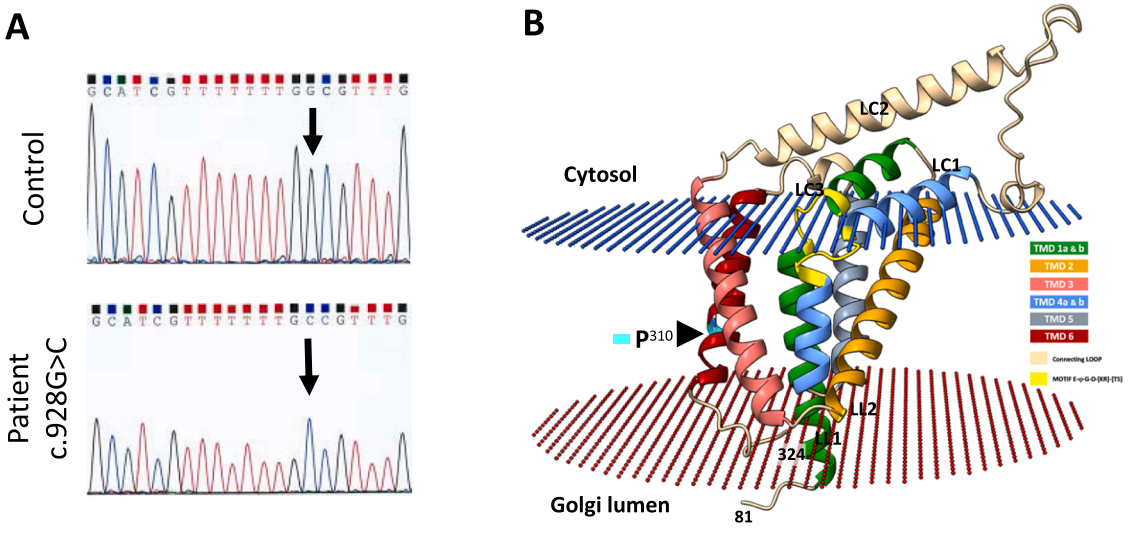

Fig. 2. Identification of a novel TMEM165 variant

A. Sequencing results of TMEM165 in control (top) and patient (bottom). The black arrow highlights the change leading to the c.928G>C;p.Ala310Pro variant. **B.** Ribbon diagram of the AlphaFold2-predicted structure of D80-TMEM165 with the variant A310P. The model is represented in a flat lipid bilayer, as calculated by the PPM 2.0 Web Server of the OPM (Orientation of Proteins in Membranes) database (see Material and Methods). The blue and red disks indicate the surfaces of the hydrophobic layer at the cytosolic and Golgi lumen sides, respectively. The right-side insert indicates the colors used to identify the predicted TMD helices and loops, and the positions of the E-Φ-G-D-[KR]-[TS] motifs (in yellow). The position of P^{310} is indicated in cyan with a black arrow.

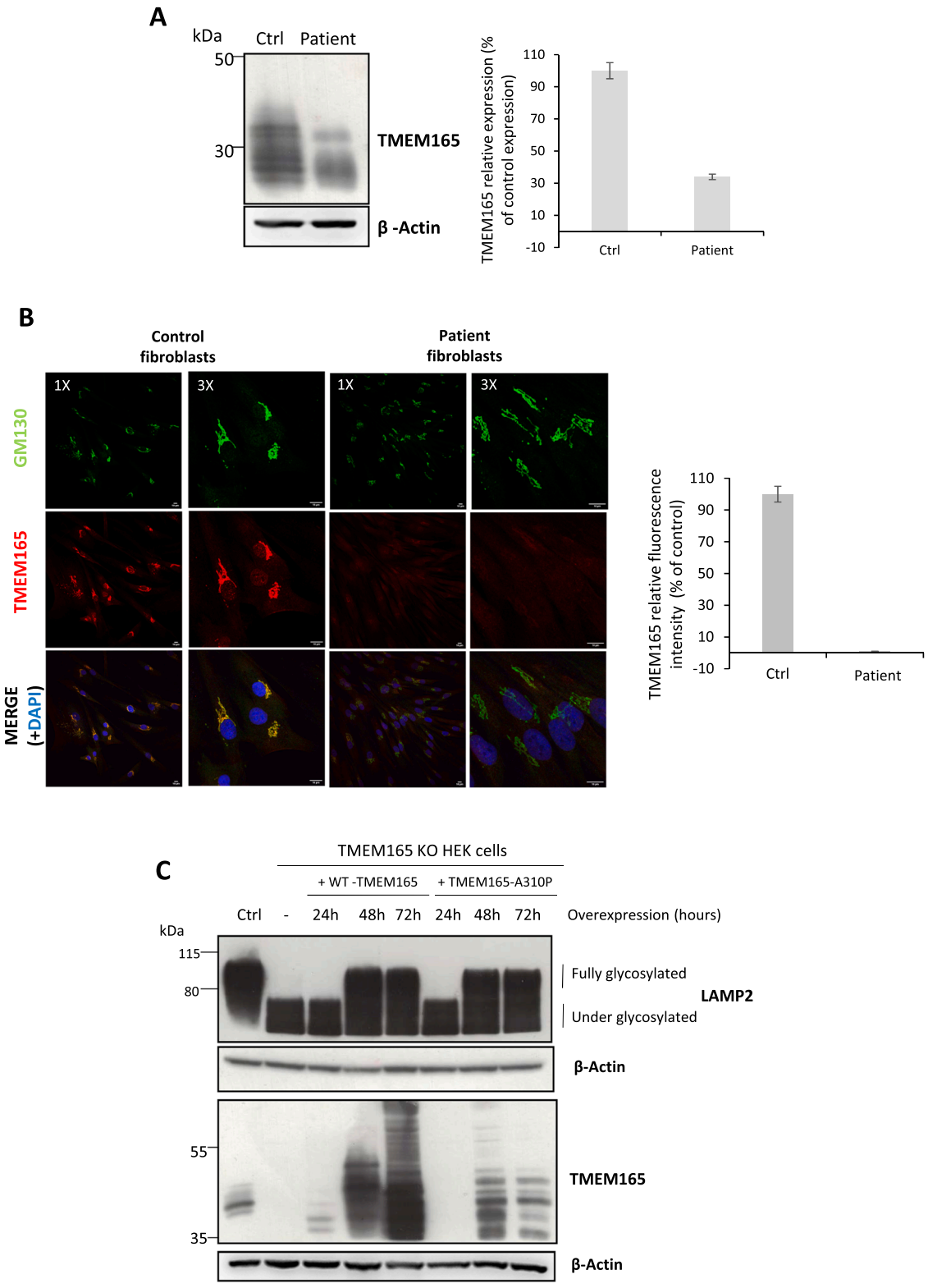

Fig. 3. Expression and functionality of TMEM165-A310P

A. Western-blot analysis of TMEM165 in control or patient skin-derived fibroblasts. The graph on the right represents the quantification of TMEM165-associated signal. B. Immunofluorescence confocal images of control or patient fibroblasts. TMEM165 signal is in red, the green signal is GM130, a Golgi marker, and cells were stained with DAPI (blue) before acquisition. For each condition, 1X or 3X images are shown. The quantification of the red TMEM165-associated signal is shown in the graph on the right. C. Western-blot and immunostaining of LAMP2 and TMEM165 in control cells, TMEM165 KO HEK cells, and TMEM165 KO HEK cells overexpressing wt-TMEM165 or TMEM165-A310P for 24, 48 or 72 hours. The glycosylation state of LAMP2 is indicated on the right.

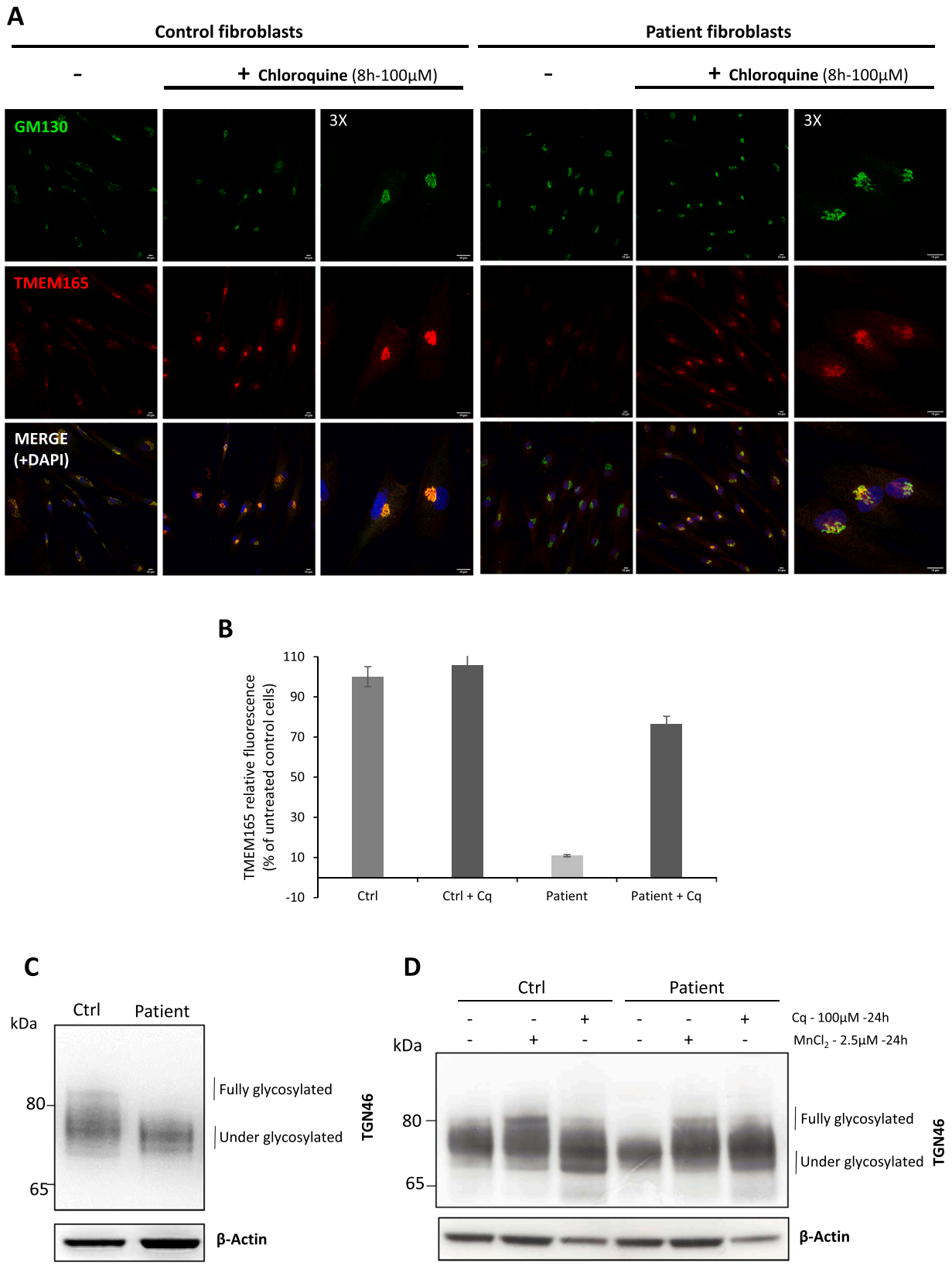

Fig. 4. TMEM165-A310P is rescued by a chloroquine, and manganese rescues the associated glycosylation defects

A. Immunofluorescence confocal imaging of control and patient fibroblasts. Cells were treated or not with 100 µM of chloroquine (Cq) for 8 hours before fixation and immunostaining of TMEM165 (red) and GM130, used as a Golgi marker (green). Nucleus were stained with DAPI (blue). B. Quantification of TMEM165-associated signal in the confocal images shown in (A). C. TGN46 Western-blot analysis in control or patient fibroblasts. The glycosylation status of TGN46 is indicated on the right. D. TGN46 Western-blot analysis in control or patient fibroblasts, previously treated for 24 hours with 100 µM of Cq or 2.5 µM of $MnCl_2$. Glycosylation status of TGN46 is indicated on the right.

the observed general glycosylation abnormalities in TMEM165 KO cells have been reported several times.[5,6,24] According to our results, we then wondered whether $MnCl_2$ supplementation, as well as Cq treatment, could possibly rescue the glycosylation in the patient's fibroblasts. To tackle this point, the migration profile of TGN46, used as a *O*-glycosylation marker[5] was followed in control and patient fibroblasts and showed an altered profile with higher gel mobility, thus demonstrating a defect in mucin-type *O*-glycosylation (Fig. 4C). The LAMP2 glycosylation defect was also investigated in patient fibroblasts but did not show any impairments (data not shown). Then, patient and control fibroblasts were treated with 2.5 μM $MnCl_2$ or 100 μM Cq for 24h and TGN46 migration profile was again followed by immunoblotting. Although $MnCl_2$ and Cq treatments had no effects on the TGN46 migration profile in control fibroblasts, these combined treatments clearly slowed down the electrophoretic gel mobility of TGN46 in patient fibroblasts arguing for the suppression of the *O*-glycosylation defect (Fig. 4 D). No differential expression level of TMEM165 in patient cells was observed followed the different treatments and importantly, D-galactose supplementation alone had no effects on TGN46 glycosylation (data not shown). Altogether, these results demonstrate the efficacy of these two different treatments on the suppression of the observed TGN46 associated *O*-glycosylation defects.

Effects of manganese therapy on overall glycosylation and other biochemical parameters

Given the young age of the patient, we started treatment with manganese and D-Gal. The treatment was started at the age of 11 months the 04/04/2022 with galactose and manganese introduced in a progressive way: galactose 0.5 g/kg/d then 1 g/kg/d, then 1.5 g/kg/d by steps of 6 weeks (Fig. 5A); manganese element 2 mg/d for 4 months (weight 7 kg) (using manganese sulphate monohydrate salt, MnSO4. H2O in magistral preparation) then 12 mg/d during 3 months, 30 mg/d during 1.5 months then 10 mg/kg/d. At 2 years old, after one year of treatment, she was receiving galactose 1.5 g/kg/d and Mn element 90 mg/d (Fig. 5A). A scheme illustrating the detailed timeline of the treatment is shown in Fig. 5A, as well as the samples analyzed. Several glycosylation serum markers were thoroughly followed. *N*-glycosylation was markedly improved both by serum N-glycomic profiling and Tf analysis to become undistinguishable from the control for S8-S10 samples (Fig 5 and supp Fig. 2). Regarding other glycosylation pathways, apoC-III and bikunin results contrast with those obtained for Tf as the rescue of the aberrant glycosylated forms was belated (S9 and S10) (Fig. 5C-D). However, a complete rescue was observed for both apoC-III and bikunin after 353 days of treatment. This shows that manganese and D-Gal therapy fully rescues all the different types of glycosylation. However, the observed differential kinetic of rescue argues for a dose-dependent effect.

Biochemical parameters were also normalized along the course of the treatment (Supp Table 1). Aspartate transferase (AST) and Alanine Transaminase (ALT) levels rapidly improved from the start of treatments but did not fully normalize (Fig. 6A). Antithrombin and Protein C levels normalized rapidly to reach normal values when treatments were at full dose. Factor XI levels also fully normalized and protein S level almost completely did when treatments were at full dose (Fig. 6A).

Effects of manganese therapy on clinical manifestations

Due to the quasi-complete rescue of the glycosylation, clinical features were also scrutinized along the course of the treatment. At 3 months after the beginning of the treatment, there was no improvement in the patient's weight and enteral nutrition was started by nasogastric tube and then by gastrostomy. The patient gained weight as soon as the calories were increased. After one year of treatment (i.e., at the age of 2 years), the patient maintained a moderate psychomotor delay with developmental scores identical to those achieved at the age of 12 months before treatment. The patient then continued to progress at her own pace. The liver remained the same size (hepatic arrow measured at 94 mm on ultrasound). On a positive note, the patient's digestive symptoms initially present, such as the diarrhea, completely disappeared. Skeletal radiographies performed 1 year after the onset of the treatment showed the persistence of bone demineralization, with the appearance of new vertebrae collapses compared to that observed before treatment (Fig. 6B). Encouragingly though, at the last evaluation of the patient (18 months of treatment), a stability of the vertebral collapse was observed (data not shown).

Effects of manganese therapy on serum and urine manganese levels

Serum and urine manganese levels were also followed (Fig. 7). Serum manganese levels, which were 8.2 nmol/L (NR: 5.5-18 nmol/L) before treatment, were 9.1 nmol/L on 2 mg/d of Mn treatment, and then remained at the upper limit of normal (between 18 and 21 nmol/L) after the increase of MnSO4 dose to 30 mg/d, without increasing further at later increases to 70 and 90 mg/d. Importantly, a marked increase in serum manganese level was seen followed slight galactose increase (S6 to S7) while the Mn administration was kept to 2 mg Mn element/d. Urine manganese levels steadily increased after the dosage increase to 30 mg/d of Mn element (Fig. 7A) arguing for an important urinary excretion. Brain MRI was performed at 12 months old and did not show any manganese accumulation in the basal ganglia.

Discussion

The identification of TMEM165-CDG patients in 2012 opened a completely new field of investigations aiming at understanding the impacts of metal ion homeostasis in glycosylation process.[3–6] TMEM165 deficiency leads to a strong Golgi Mn^{2+} decrease and a concomitant cytosolic Mn^{2+} increase.[25] Many results demonstrate that alterations in Golgi Mn^{2+} homeostasis are at the origin of the glycosylation defects observed in TMEM165-deficiency, leading to the severe clinical presentation characterized by dwarfism, skeletal malformations and psychomotor retardation. TMEM165-CDG leads to hypogalactosylation of all the different glycosylation subtypes investigated (*N*- and *O*-glycans; glycolipids; GAGs) that likely contributes to the unique clinical phenotype of the TMEM165-CDG patients.

We here report a novel TMEM165-CDG patient with a previously undescribed pathogenic TMEM165 variant. Clinical features for this young patient include slight developmental delay, digestive symptoms, hemostasis defects, retinoschisis and bone impairment. The comparison with the symptoms observed in other TMEM165-CDG patients is difficult given the very young age of this patient. In the present case, a profound alteration of all the Golgi glycosylation types (*O*-, and *N*-glycans, and GAGs) mostly characterized by undergalactosylation was observed, which is fully reminiscent of the other characterized TMEM165-CDG patients. Remarkably, the glycosylation defects appeared simultaneously with or after to breastfeeding cessation. Although not fully elucidated, this has already been observed in another TMEM165-CDG patient with changes in glycosylation patterns over the first postnatal weeks. This highly suggests the presence of protective factors in maternal milk.

The A310P variant for which the patient is homozygous encodes an unstable protein whose degradation is inhibited by chloroquine. Interestingly this variant does not seem to affect the manganese import function of the protein, as the overexpression of the mutated form in TMEM165 KO cells rescues LAMP2 glycosylation. Why this pathogenic variant leads to a higher lysosomal degradation is not solved yet. Overall, our results indicate that the observed Golgi glycosylation defects arise from a complete lack of TMEM165 in the Golgi due to its higher lysosomal degradation rate.

This prompted us to consider manganese supplementation as a treatment for patients with TMEM165-CDG. Two SLC39A8-CDG

A

Treatment

Date	07/01/2021	01/13/2022	03/17/2022	04/04/2022	06/14/2022	10/10/2022	12/20/2022	03/23/2023	06/11/2023
Age	2m	9m	11m	11m	1y 2m	1y 6m	1y8m	1y11m	2y2m
Weight	4 kg (-2.19 DS)	7,10 kg (-1.40 DS)	7 kg (-2.06 DS)	7 kg (-2.06 DS)	7 kg (-2.62 DS)	7,4 kg (-3 DS)	7.440 kg (-3.16 DS)	10.845kg (-0.5DS)	11.70 kg (-0.22 DS)
Height	/	65,7 cm (-1.32 DS)	67,5 cm (-1.73 DS)	67,5 cm (-1.73 DS)	68 cm (-2.81 DS)	72 cm (-3 DS)	72 cm (-3.3 DS)	78cm (-2DS)	80.5 cm (-1.83 DS)
D-Galactose				**4 g/d** for 6 weeks, **8g/d** for 6 weeks then **12g/d**	**12 g/d**	**12 g/d**	**12 g/d**	**12 g/d**	**12 g/d**
Dose D-Gal g/kg/d				0.57 then 1.14 then 1.71	1.71	1.62	1.61	1.11	1.02
Manganese element using manganese sulphate monohydrate salt, MnSO4.H2O				**2mg/d**	**2mg/d**	**30 mg/jour** for 6 weeks then **70 mg/jour**	**70 mg/d**	**90 mg/d**	**90 mg/d**
				0.28	**0.28**	**4.05 and 9.45**	**9.4**	**8.33**	**7.69**
Number of days of treatment				**0**	**71d**	**189d**	**260d**	**353d**	**433d**
Samples Analyzed	**S1** **S2: 08/24/21** **S3: 10/11/21**	**S4**	**S5**		**S6** **S7: 07/08/22**	**S8**	**S9**	**S10**	**S11**

B

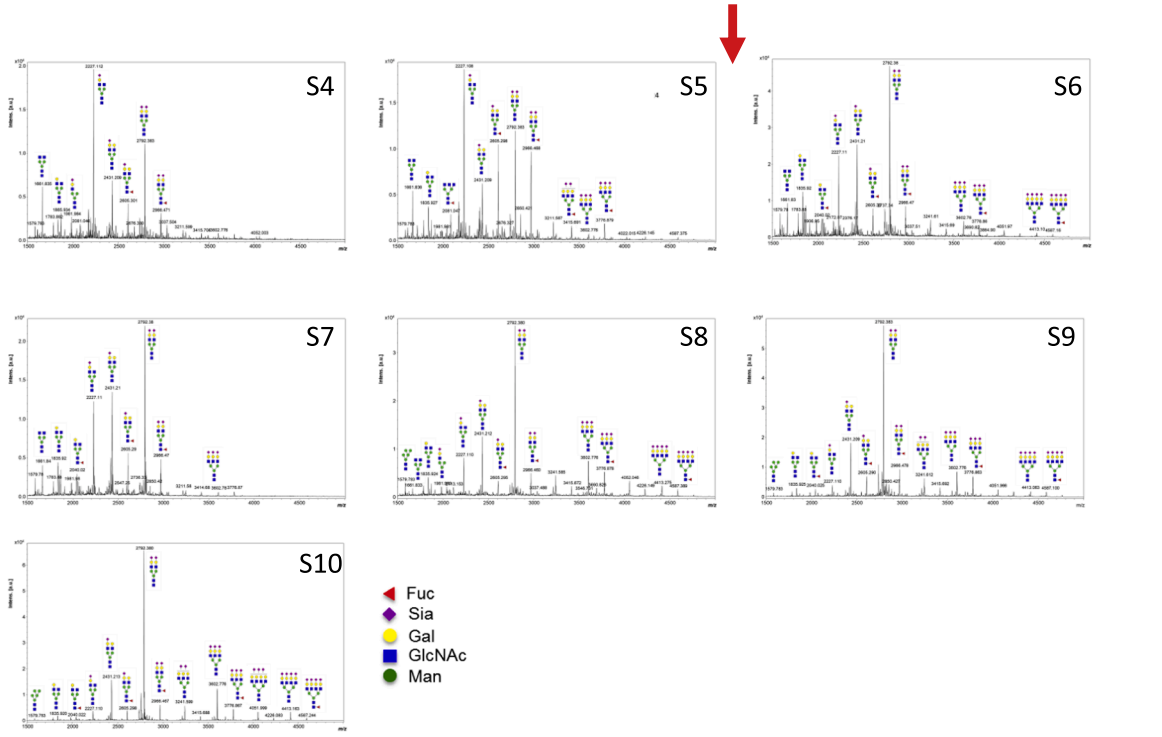

C

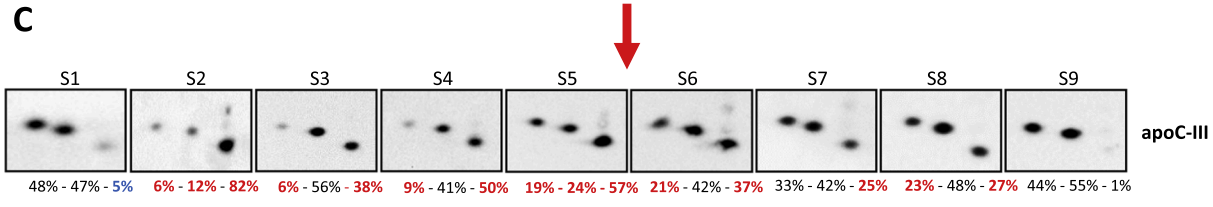

D

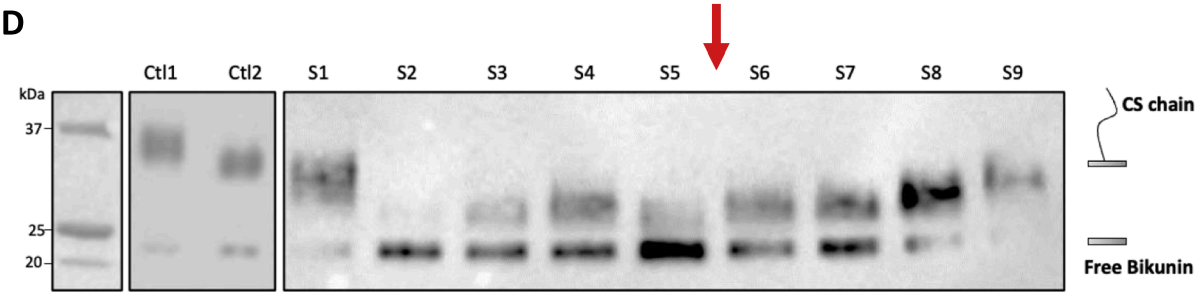

(caption on next page)

Fig. 5. Effects of manganese and D-Gal therapy on *N*-glycome, apoc-III and bikunine profiles
A. Table representing the timeline of the patient's care. The age, weight and height of the patient is indicated for each date. D-Gal and manganese doses are indicated. S1 to S10 represent the samples collected for further analysis as well as the collection date. B. Total serum *N*-glycome analysis by MALDI-TOF MS in all patient samples, from S4 to S10 (the symbols used to depict monosaccharides are as mentioned in the legend of Fig. 1). The starting point of treatment is highlighted by a red arrow between spectra S5 and S6. C. Two-dimensional western blot of serum apoC-III in patient's samples from S1 to S10. The age corresponding to the sample collect time is indicated on top. The treatment start is highlighted by a purple arrow. The % under the spots correspond to the glycosylation status of each apoC-III glycoforms. The first % corresponds to the bi-sialylated (2 sialic acids) apoC-III glycoform, the second % corresponds to the mono-sialylated (one sialic acid) glycoform and the last % corresponds to the aglycosylated form (without any glycan chain). The abnormal % values are indicated in red. D. Bikunin western-blot analysis in controls (Ctl1, Ctl2) and patient's samples from S1 to S10 (corresponding ages are indicated on top). The bikunin glycosylation (by a CS chain) is schematized on the right.

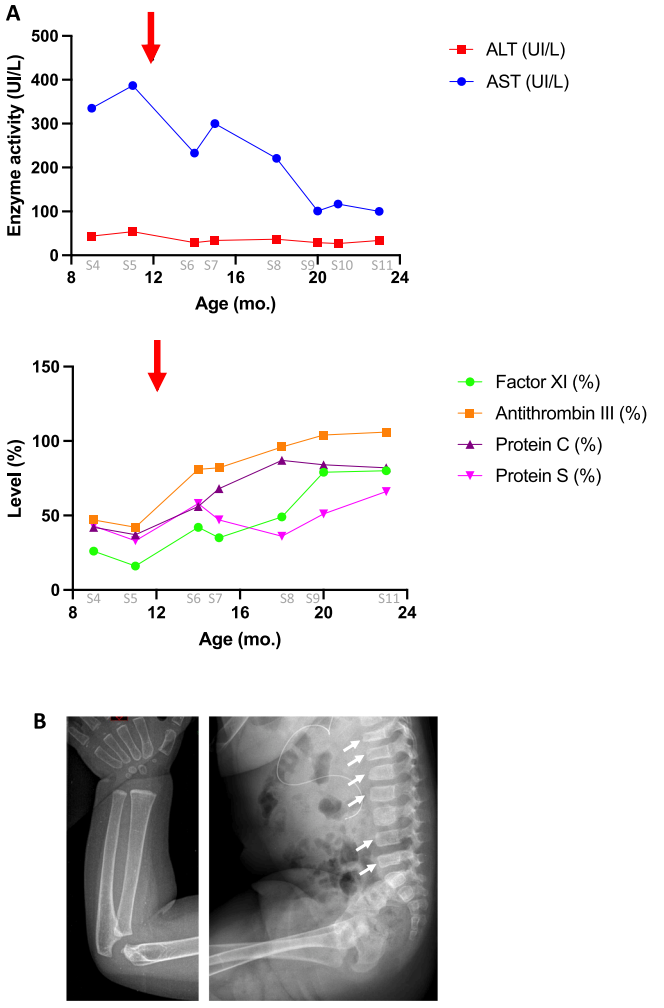

Fig. 6. Effects of manganese and D-Gal therapy on biochemical and clinical parameters
A. Liver function test results (top) and coagulation test results (bottom) of the patient. Red arrow indicates the introduction of treatment. Patient age and sample numbers are indicated below the *x* axis. Legends on the right of figures indicate the normal ranges (NR) for each parameter. B. In the follow up at 1 year after manganese, left arm radiography (left) shows persistence of bone demineralization and spine radiography (right) shows appearance of new vertebral collapses (complete arrow).

patients have already been treated with 15 and 20 mg Mn/kg/d, and such treatment led to remarkable biochemical and clinical improvements.[26–28] However, the required daily-dose for a complete correction of glycosylation was found as high as 20mg/kg/d due to the nature of the SLC39A8 defect that impairs cellular manganese uptake. For comparisons at two years old our patient is only receiving 7.69mg/kg/d. This dose is for the moment sufficient to fully rescues the different glycosylation types but can quickly turn out to be insufficient

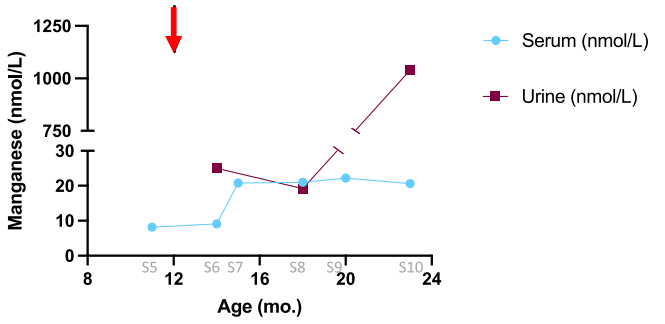

Fig. 7. Serum and urine manganese levels in treated patient
Red arrow indicates the introduction of treatment. Patient age and sample numbers are indicated below the *x* axis.

when the patient will gain weight.

As D-Gal supplementation had already been shown to be beneficial in two TMEM165-CDG patients,[13] a combined D-Gal and Mn2+ oral treatment was introduced in a progressive way to reach a daily dose of 12 g/d of D-Gal and 90 mg/d of Mn element. Remarkably, a complete rescue of all different Golgi glycosylation pathways was seen throughout the course of the treatment to reach profiles similar to that of controls. Of note, differential effects of the treatment are seen on the different Golgi glycosylation types. The observed manganese increases in the serum following increased D-Gal supplementation, although oral manganese intake was not increased, raises intriguing questions. Although the molecular mechanism is truly unknown, this observation asks about the galactose effect on manganese level. If confirmed, the galactose effects on glycosylation observed by us and others could result from the manganese effect.

This complete glycosylation rescue was accompanied by a complete recovery of coagulation parameters, a quasi-normalization of liver function tests, and a clear decrease in CK activity, which remained a little above the normal range. In the two patients previously treated by D-Gal only, the effect on these parameters was more contrasted: ALT was improved only in one patient, while in both patients coagulation parameters did not fully recover and CK activity remained much above the reference range (Supp Fig. 1). However, and quite surprisingly, we did not observe a clinical improvement yet, except for the digestive features that disappeared. We suspect that the duration of the treatment is not sufficient. Clinical improvement has been seen after 476 days of manganese therapy in SLC39A8-CDG.[28] A longer follow up of the patient is required to make a conclusion. Altogether, our results are of importance for the potential treatment of future patients and suggest to use high doses of manganese.

Although manganese supplementation appears as a powerful and promising therapy for TMEM165-CDG patients, the main obstacle remains the possible toxicity of manganese. Indeed, as to sustain the manganese effects on glycosylation during child growth, manganese doses will need to be increased. Importantly, during the course of the treatment, we did not detect any symptoms of manganese toxicity. The manganese concentrations in body fluids have been followed and remain normal in blood (higher normal reference range) but

significantly increased in urine, although manganese excretion via urine is normally physiologically low. In general population, whole blood, serum, and urinary manganese concentrations are below 15 ug/L.[29] It is important to note that neither serum or urine manganese concentrations are efficient biomarkers in determining tissue bioaccumulation and the risk of toxicity.[30]

In summary, we identified and characterized a novel homozygous pathogenic TMEM165 variant in a very young patient and proposed for the first time a combined manganese and D-gal therapy for TMEM165-CDG. Although the supplementation improved laboratory glycosylation, hepatic function and coagulation assays, the clinical phenotype only showed stabilization, without major signs of improvement. We did not observe any signs of manganese toxicity but a close follow-up in the coming years is required to exclude side effects and keep track of clinical improvements.

Background

TMEM165 is a Golgi Ca^{2+}/ Mn^{2+}: H^{+} antiporter crucial to import manganese for Golgi glycosylation enzymes. TMEM165 defects belong to Congenital Disorders of Glycosylation (CDG) for which no treatment exists. Our previous work has shown that *in cellulo*, manganese supplementation could rescue glycosylation.

Translational

Manganese supplementation to an 11 months-old TMEM165-CDG patient with a novel variant suppressed the glycosylation abnormalities and improved biochemical parameter.

Acknowledgments

This work was supported by the French National Agency (ENIGMncA project, ANR-21-CE14-0049-01 to F.F.), The IRP CNRS GLYCOCDG to F. F. and the ERA-Net for Research on Rare Diseases (ERARE118-117 - EUROGLYCAN-omics) to F.F. Z.D. was supported by a fellowship from Région Hauts-de-France and Lille university. This research was made possible through access to the data generated by the France Genomic Medicine Plan 2025. This work was supported by Commissariat a` l'Energie Atomique et aux Energies Alternatives and the MetaboHUB infrastructure (ANR-11-INBS-0010) (F. Fenaille, S. Cholet). We thank Dr. Olivia Baylet-Fernandez (pediatrician), Dr. Bamberger (pediatrician), Dr Pinto (endocrinologist), Dr Dehoux (nephrologist), Dr Girard (hepatologist), Pr Cormier-Daire (genetician), Manon Tessier (psychomotrician), Clarisse Duchon (neuropsychologist), Pr Borgel (hematologist) for their help in patient management and Mounira Zerguini (ARC). All authors have read the journal's authorship agreement and policy on disclosure of potential conflicts of interest and they declare no conflict of interests.

Supplementary materials

Supplementary material associated with this article can be found, in the online version, at doi:10.1016/j.trsl.2023.11.005.

References

1. Monticelli M, et al. Congenital disorders of glycosylation: narration of a story through its patents. *Orphanet J Rare Dis*. 2023;18:247.
2. Jaeken J, et al. Familial psychomotor retardation with markedly fluctuating serum prolactin, FSH and GH levels, partial TBG-deficiency, increased serum arylsulphatase A and increased CSF protein: a new syndrome?: 90. *Pediatr Res*. 1980; 14:179. -179.
3. Foulquier F, et al. TMEM165 deficiency causes a congenital disorder of glycosylation. *Am Hum Genet*. 2012;91:15–26.
4. Zeevaert R, et al. Bone dysplasia as a key feature in three patients with a novel congenital disorder of glycosylation (CDG) Type II due to a deep intronic splice mutation in TMEM165. *JIMD Rep*. 2012;8:145–152.
5. Durin Z, et al. Differential effects of D-galactose supplementation on golgi glycosylation defects in TMEM165 deficiency. *Front Cell Dev Biol*. 2022;10, 903953.
6. Potelle S, et al. Glycosylation abnormalities in Gdt1p/TMEM165 deficient cells result from a defect in Golgi manganese homeostasis. *Hum Mol Genet*. 2016;25: 1489–1500.
7. Lebredonchel E, et al. Dissection of TMEM165 function in Golgi glycosylation and its Mn2+ sensitivity. *Biochimie*. 2019;165:123–130.
8. Brasil S, et al. CDG therapies: from bench to bedside. *Int J Mol Sci*. 2018;19:E1304.
9. Ondruskova N, Cechova A, Hansikova H, Honzik T, Jaeken J. Congenital disorders of glycosylation: Still "hot" in 2020. *Biochim Biophys Gen Sub*. 2021;1865, 129751.
10. Witters P, et al. Clinical and biochemical improvement with galactose supplementation in SLC35A2-CDG. *Genet Med*. 2020;22:1102–1107.
11. Wong SY-W, et al. Oral D-galactose supplementation in PGM1-CDG. *Genet Med*. 2017;19:1226–1235.
12. Witters P, Cassiman D, Morava E. Nutritional therapies in congenital disorders of glycosylation (CDG). *Nutrients*. 2017;9:1222.
13. Morelle W, et al. Galactose supplementation in patients with TMEM165-CDG rescues the Glycosylation defects. *J Clin Endocrinol Metabol*. 2017;102:1375–1386.
14. Parente F, Ah Mew N, Jaeken J, Gilfix BM. A new capillary zone electrophoresis method for the screening of congenital disorders of glycosylation (CDG). *Clin Chim Acta*. 2010;411:64–66.
15. Bruneel A, et al. Complementarity of electrophoretic, mass spectrometric, and gene sequencing techniques for the diagnosis and characterization of congenital disorders of glycosylation. *Electrophoresis*. 2018;39:3123–3132.
16. Goyallon A, Cholet S, Chapelle M, Junot C, Fenaille F. Evaluation of a combined glycomics and glycoproteomics approach for studying the major glycoproteins present in biofluids: application to cerebrospinal fluid. *Rapid Commun Mass Spectrom*. 2015;29:461–473.
17. Ceroni A, et al. GlycoWorkbench: a tool for the computer-assisted annotation of mass spectra of glycans. *J Proteome Res*. 2008;7:1650–1659.
18. Two-dimensional gel electrophoresis of apolipoprotein C-III and other serum glycoproteins for the combined screening of human congenital disorders of O- and N-glycosylation - Bruneel - 2007 - PROTEOMICS – clinical applications - Wiley online library. https://onlinelibrary.wiley.com/doi/abs/10.1002/prca.200600777.
19. Haouari W, et al. Serum bikunin isoforms in congenital disorders of glycosylation and linkeropathies. *J Inherit Metab Dis*. 2020;43:1349–1359.
20. Jumper J, et al. Highly accurate protein structure prediction with AlphaFold. *Nature*. 2021;596:583–589.
21. Legrand D, et al. New insights into the pathogenicity of TMEM165 variants using structural modeling based on AlphaFold 2 predictions. *Comput Struct Biotechnol J*. 2023;21:3424–3436.
22. Spatial arrangement of proteins in planar and curved membranes by PPM 3.0 - Lomize - 2022 - protein science - Wiley online library. https://onlinelibrary.wiley.com/doi/10.1002/pro.4219.
23. Mirdita, M. et al. ColabFold - Making protein folding accessible to all. 2021.08.15.456425 Preprint at https://doi.org/10.1101/2021.08.15.456425 (2022).
24. Houdou M, et al. Involvement of thapsigargin- and cyclopiazonic acid-sensitive pumps in the rescue of TMEM165-associated glycosylation defects by Mn2. *FASEB J*. 2019;33:2669–2679.
25. Vicogne D, et al. Insights into the regulation of cellular Mn2+ homeostasis via TMEM165. *Biochim Biophys Acta Mol Basis Dis*. 2023;1869, 166717.
26. Choi E-K, Nguyen T-T, Gupta N, Iwase S, Seo YA. Functional analysis of SLC39A8 mutations and their implications for manganese deficiency and mitochondrial disorders. *Sci Rep*. 2018;8:3163.
27. Park JH, et al. SLC39A8 deficiency: a disorder of manganese transport and glycosylation. *Am J Hum Genet*. 2015;97:894–903.
28. Park JH, et al. SLC39A8 deficiency: biochemical correction and major clinical improvement by manganese therapy. *Genet Med*. 2018;20:259–268.
29. Chen P, Bornhorst J, Aschner M. Manganese metabolism in humans. *Front Biosci (Landmark Ed)*. 2018;23:1655–1679.
30. Zheng W, Fu SX, Dydak U, Cowan DM. Biomarkers of manganese intoxication. *Neurotoxicology*. 2011;32:1–8.